Chapter 11

The SemiLoof Shell Element

Bruce M. Irons

11.1 Introduction and motivation

This chapter is intended as the definitive account of 'SemiLoof'. It is hoped that, while researchers will find all their needs satisfied here, the typical user will merely flirt with this chapter, content that the element is trouble-free and easy to use. For SemiLoof is by far the most complex isoparametric element ever to enter service in industry. The author has been thinking about the difficult problems of engineering shells for over ten years. This, then, probably represents the final stage in his quest, a quest motivated by a deep dissatisfaction with almost all known thin shell elements. The following list of requirements neatly summarizes this dissatisfaction.

(1) The element should be a direct stiffness element, because many millions of pounds have been spent on general purpose programs which accept only such elements.
(2) The element should be mixable—in the strict sense of the patch test[1]—with other triangular and quadrilateral elements of uniform thickness. (SemiLoof is the first of the Ahmad family to pass this test as a quadrilateral, mixed with triangles and with a very special beam element recently coded by Albuquerque.[2])
(3) A patch as above, but comprising elements of any shape, must accept any rigid-body motion exactly.
(4) Very thin shell problems with linear generators sometimes give exceptionally high flexibilities, although the modes involved are usually unloaded. The resulting difficulties, both in geometric modelling and in equation solving, may tax the best elements. Shell problems are difficult, especially when the shell is so thin that the bending stiffness is negligible compared with the membrane stiffness, and when in addition one of the principal curvatures is positive, the other negative or zero.
(5) Most engineering shells have sharp corners and multiple junctions. Accordingly, the element must model these, without pathological exceptions, and without additional complications depending on the nature of the multiple junction.
(6) Whatever basic model is chosen, it should be implemented as a shape function routine, a black box whose details need not concern the user and which encapsulates all the complications such as transformations, sign conventions, etc. In this way the originator can most effectively ensure that his program is easily and correctly implemented in the first place and that any exotic element

properties which are needed later—inevitably at short notice—can be added with little effort. (Numerical integration will make short work of, for example, some unplanned kind of force, e.g. force arising from gyroscopic action, or some electrical effect.)

Note that the popularity of the isoparametric elements is due in no small degree to the presence of a simple shape function routine which, once checked and documented, can safely be given many tasks. We are thinking here of a more complex routine, but the payoff remains.

(7) The shape function routine itself should be accessible to the maintenance programmer, with transparent coding, adequate documentation and ample optional printout.

(8) The shape function routine must be foolproof and easy to use. (For example, the numerical procedure may be different the first time it encounters a new element, but we should not have to inform the computer of this fact.)

(9) Again, it is a kind gesture to the final user to provide good diagnostics. The most convenient place for many of the diagnostics is within the shape function routine. (Little harm will be done if we duplicate certain diagnostic checks which are present in some, but not all, finite element systems.)

(10) Many programmers try to maximize the number of subroutine segments. Perhaps we have a case here for the opposite philosophy. The main tasks in incorporating a foreign subroutine are to harmonize the housekeeping and to reorganize the selective loading of the subroutines into core. The author takes the view that a prospective user would prefer to be given a few subroutines, even if some are quite lengthy.

(11) The element should not be temperamental in performance. For example, it should be free from hazards like low rank. (It remains a burning question whether we should speak of 'convergence' at all, so long as certain assemblages of elements can experience spurious mechanisms. In practice this is usually linked with the question of whether the rank of the element stiffness matrix is less than (number of nodal degrees of freedom) minus (feasible rigid-body motions), which tests whether a single element can have spurious mechanisms.)

(12) Extreme accuracy is never needed, but a very coarse mesh should not give unreasonable results. According to the general consensus, stresses that vary linearly will best satisfy the needs of engineers. We shall always be interested in that mesh which gives barely acceptable errors, say ± 5 per cent.

11.2 SemiLoof nodal configuration

From the user's point of view, the nodal configuration shown in Figure 11.1 is difficult to fault—it seemed the most attractive of the possibilities listed in Reference 1. At corners and at midsides we have u, v, w, the deflections in global x, y, z directions. This would be enough for a membrane shell, but it cannot prevent hinging in a shell with bending stiffness. To provide a semblance of $C^{(1)}$ conformity, we introduce the normal rotations at the two Gauss points along each side. The 32 degrees of freedom should be sufficient to define linear

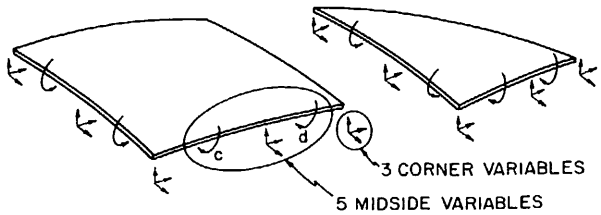

Figure 11.1 Diagram showing the nodal variables for the SemiLoof quadrilateral and triangle shell element

stress fields, both in membrane and in bending action. For the programming logic, we group the five variables along a side as 'midside' variables, as if they all operated at the midside node. The sign convention—which need very seldom concern the user—depends on the identification numbers of the adjacent corner nodes, say N_1 to the left of c and d in Figure 11.1, and N_2 to the right. If $N_2 > N_1$, then the rotations c and d have the sense as shown, i.e. a right-hand screw from N_1 towards N_2; also c precedes d. Conversely, if $N_2 < N_1$, then c and d must be interchanged and their signs reversed. (Observe that N_1 and N_2 can never be equal, because they identify the nodal coordinates of two different nodes.)

We shall now describe a particular implementation using this nodal configuration. The reader should carefully distinguish between those characteristics which result from the nodal variables—in our opinion almost entirely favourable—and those more controversial features which result from our formulation.

11.3 Precursors of SemiLoof

The remainder of the chapter gives an introduction not only to SemiLoof (our version) but also to the techniques which characterize the second generation of isoparametric elements. No formulation emerges from a historical vacuum, and SemiLoof has an especially long ancestry; consequently its history reflects fairly comprehensively the present state of the art.

11.3.1 Loof nodes

A plane problem may be solved using *Loof nodes*, which are placed at the two Gauss points along each edge of an element, as in Figure 11.2. It is necessary

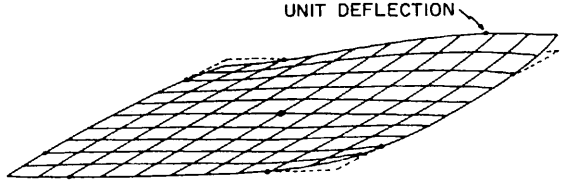

Figure 11.2 Perspective view of a Loof shape function, represented as a vertical displacement

to add the ninth central node: the pursuit of the shape functions is described in Reference 3. In the absence of corner connections, it is impossible to have even $C^{(0)}$ between elements.

However, the nonconformity tends to be $P_2(\xi)$, the Legendre polynomial with zeros at the two Gauss points, whose integral and first moment in ξ vanishes. (Here ξ is the local variable which goes from -1 to 1 along the edge in question.) We consider now a *patch test*, with stress assumed constant. Any perturbation from this state will induce discontinuities of displacement across element boundaries. If these jumps were to vary as $P_2(\xi)$, where ξ varies linearly along the edge, then they would involve no work. In fact, the jumps can vary as cubics in ξ, but cubics with zeros at the two Gauss points. Again, in a field of uniform stress, a perturbation that would introduce jumps does virtual work, which can be calculated exactly using 2-point Gauss quadrature, and is therefore zero. Provided the rank is adequate, then, the test is passed.

Historical note H. W. Loof almost certainly invented such nodes; see the early date of his contribution.[4] This described a technique for using exact solutions within each element, of quite high order, which would not automatically conform. Given that a certain degree of nonconformity between elements was unavoidable, he tried to minimize its effects by using the Lobatto points as nodes along each side, as in Figure 11.3. The argument was that with six such nodes along each side, for example, one might expect a sextic variation of nonconformity, it being zero at the six nodes—or 'collocation points', as he preferred to call them. But this would be a very special sextic, on account of the positioning of the 'collocation points', in that the nonconformity multiplied by *any cubic whatsoever* would integrate to zero.

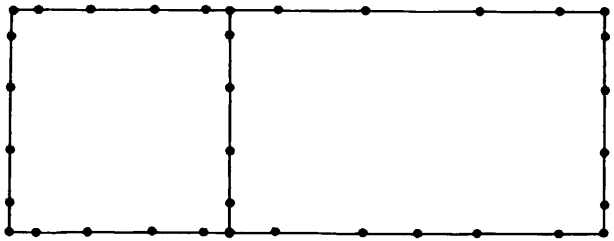

Figure 11.3 When rectangular elements are connected at Lobatto points, as in Loof's original calculations, any nonconformity present is made as harmless as possible by the positioning of the nodes

The virtual work generated by the nonconformity may be expressed as such an integral. This virtual work corresponds to a generalized force tending to cause nonconformity. Nowadays we should express such thoughts somewhat more precisely, as above, in terms of the patch test. Incidentally, although in SemiLoof we have eight Loof nodes on the perimeter, it appears to be intrinsically impossible to satisfy a patch test with linearly varying stresses.[5] However, SemiLoof does pass the test with linear bending stresses, in a mesh of parallelograms.

11.3.2 Visser's element

Visser's element,[6] amongst others, postulates a linear variation of bending moment across each edge, as in Figure 11.4. We could, however, reformulate it in terms of the lumped moments:

$$M = (\text{moment density/inch}) \,.\, \text{d(side)}/\text{d}\xi \tag{11.1}$$

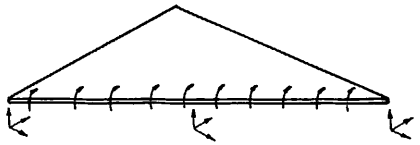

Figure 11.4 The variables of Visser's shell element relate to the displacement at the corner and midside nodes and to the linearly varying bending moments about each edge

at the two Gauss points, so that any work would be the sum of (M times rotation) at the two Loof nodes. Then a part-inversion[7] should give an exactly equivalent direct stiffness version, involving Loof rotations.

11.3.3 Isoparametric membrane

The isoparametric membrane of Figure 11.5 uses shape functions $N_i(\xi, \eta)$ to map into three dimensions:

$$\begin{bmatrix} x \\ y \\ z \end{bmatrix} = \sum N_i \begin{bmatrix} x \\ y \\ z \end{bmatrix}_i, \quad \begin{bmatrix} u \\ v \\ w \end{bmatrix} = \text{deflections} = \sum N_i \begin{bmatrix} u \\ v \\ w \end{bmatrix}_i$$

This is a very straightforward element. It has only one slight complication: when we compute the membrane strains they must, to have any meaning, be in the local X, Y axes in the tangent plane to the membrane. We use the

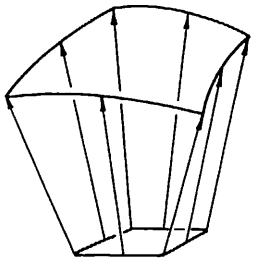

Figure 11.5 An isoparametric membrane may be regarded as a square plane element with very large initial displacements

following equation to get the X, Y derivatives of the shape functions (see Appendix to this chapter):

$$\begin{bmatrix} \partial N_i/\partial \xi \\ \partial N_i/\partial \eta \end{bmatrix} = \begin{bmatrix} \boldsymbol{\xi} \cdot \hat{\mathbf{X}} & \boldsymbol{\xi} \cdot \hat{\mathbf{Y}} \\ \boldsymbol{\eta} \cdot \hat{\mathbf{X}} & \boldsymbol{\eta} \cdot \hat{\mathbf{Y}} \end{bmatrix} \begin{bmatrix} \partial N_i/\partial X \\ \partial N_i/\partial Y \end{bmatrix} \tag{11.2}$$

Here $\hat{\mathbf{X}}$, for example, is the unit vector along the local axis X. The vector $\boldsymbol{\xi}$ represents $[\partial x/\partial \xi, \partial y/\partial \xi, \partial z/\partial \xi]$, known as a covariant base vector. We write the scalar product as, e.g. $\boldsymbol{\xi} \cdot \hat{\mathbf{X}}$.

Having computed the X, Y derivatives of the N_i we can assert, for example, that a displacement of $\mathbf{d}_i$ at the node i contributes

$$\mathbf{d}_i \cdot \hat{\mathbf{Z}} \frac{\partial N_i}{\partial X} \tag{11.3}$$

towards $\partial W/\partial X$ at the given point (ξ, η). The strains and related quantities now follow readily. Essentially the same formulae will be used for the membrane and bending stresses in SemiLoof, so we shall return to the point later.

11.3.4 The Ahmad membrane stack

The Ahmad membrane-stack[8] (for moderately thick shells) was devised at a time when vectorial arguments were conspicuously absent from finite element texts. It was implemented as an introductory exercise; its success and subsequent popularity were wholly unexpected. The idea goes back to Melosh[9] or even to Winkler's theory of thick curved beams[10] (1885) in which normal sections remain plane but not normal. This recurring theme is especially attractive in shells, for the iso-P bricks are conceptually simpler than classical shell theory.

Figure 11.6 presents the idea graphically. The 20-node brick supplies the geometry and the deformations. The eight lines normal to the shell are straight,

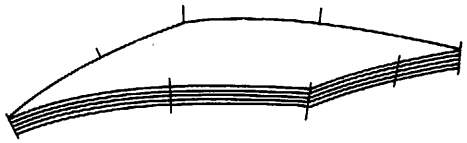

Figure 11.6 An Ahmad membrane-stack derives its bending stiffness from the differential membrane action of its component sheets. But this will be largely ineffective, unless there is some way of suppressing the lateral shear strains, i.e. slipping between the sheets

and the midside nodes on the four lines in the corners are truly central. Thus, x, y and z vary linearly with ζ at all points.

Each of the eight lines is given three deflections. u, v and w, at the mid-surface $\zeta = 0$, and two rotations normal to itself. Thus the element has 40 degrees of

freedom. Each line is rigid and a layer connects to it as if to an ordinary node. For each layer, ζ to $\zeta + d\zeta$, is an iso-P membrane of variable thickness, controlled by all eight nodal lines. Such a membrane is in a state of plane stress. Thus any strain normal to the membrane—or the absence of strain—is irrelevant, as in conventional plate or beam theory.

Elastically, we do not yet have a realistic shell. The membranes resemble the pages of a book, which can slide freely. But we have learnt how to glue the pages together, to make the book stiff in bending and impossible to read. Two techniques are in use:

(1) Ahmad added the strain energy due to the shear strains, as each membrane slides relative to its neighbours. This is initially a crude model: the shear at the upper and lower shell surfaces is small or zero in reality, except in the unusual circumstance that appreciable loads are applied to the surfaces by shear traction. We always assume in practice that the shear varies as $(1 - \zeta^2)$, as in Figure 11.7, and it follows that the normals do not remain straight when shear is present. Ahmad corrects the model whose 'normals' remain straight, by dividing the lateral shear strains by $\sqrt{(1{\cdot}2)}$. (Note that the shear γ_{XY} in the membrane is unaffected.)

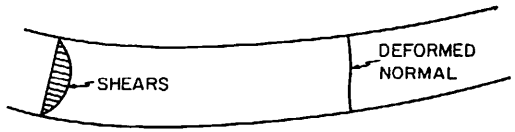

Figure 11.7 The lateral shear is not uniform across the thickness. In consequence, normals do not remain quite straight

(2) Alternatively, we can make the shear effectively zero—as it indeed is for a thin shell—by constraining it to be exactly zero at certain chosen points. We can exploit these constraints to discard certain nodal variables. The Discrete Kirchhoff Assumption is being used increasingly[11] because it sometimes produces elements with exceptionally good performance. We adopt it in SemiLoof in preference to the Ahmad technique, although it is the more difficult option.

11.3.5 Ahmad membrane-stack with 2 × 2 integration

During a careful survey of integrating rules, Too[12] observed that 2 × 2 Gaussian integration gives remarkably improved results in the quadratic stack, provided that one calculates the final stresses at the same 2 × 2 points. This observation[13,14] has never been explained, yet it has already suggested several effective innovations.

Let us ponder, why the good results are so unexpected when the plate or shell is thin. In this case, the shear strain energy applies eight virtually rigid constraints per element. Now let us consider a fine mesh, as shown in Figure 11.8,

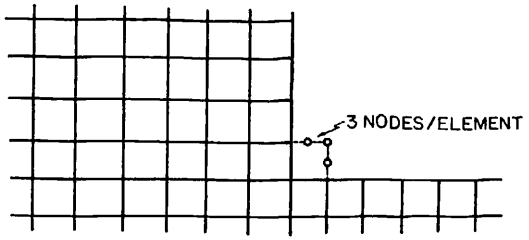

Figure 11.8 In an extensive mesh, each element tends to add three nodes on average, one corner node and two midside nodes

for an Ahmad plate element, with the lateral deflection and the two bending slopes as nodal variables. Each element adds three nodes, i.e. nine degrees of freedom. Subtracting the eight constraints, we have only one genuine kinematic degree of freedom per plate element. Yet the results are good.

Note It would be tempting to cite this as further evidence of the prodigal use of nodal variables in finite element calculations. The objective here is not to repeat an already familiar criticism, however, but merely to enquire whether we can derive some practical benefit from it.

11.3.6 The first delinquent element

The first delinquent element[15] (an approximately integrated iso-P element with Discrete Kirchhoff Assumptions) was suggested, on the one hand, by the unexpectedly good behaviour of the Ahmad stack with 2 × 2 integration and, on the other hand, by its inbuilt inefficiency. Let us consider this again from a different viewpoint. Lateral shear typically accounts for only a few per cent or less of the strain energy. In real problems, it seldom makes much difference whether we include shear or not. Yet the stack provides quadratic variation or shear with ξ or η and only linear variation of bending stresses.

So we have superfluous degrees of freedom: which eight can we profitably discard, if we choose to constrain the shears at the Gauss points to exactly zero? Figure 11.9 provides the most obvious answer. If AB were a simple beam, with

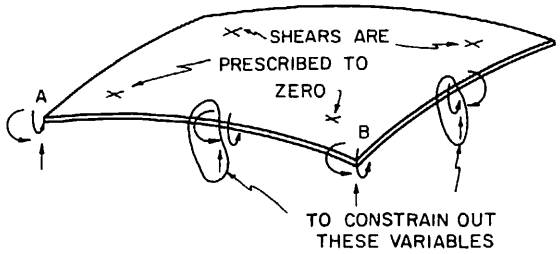

Figure 11.9 It is possible to constrain out the eight unwanted nodal variables by making zero the lateral shears at the 2 × 2 Gauss points

linear bending stress, its deformation would be adequately defined by the deflection and slope at its two ends. The deflection and slope at the centre are unnecessary. This leads us to enquire whether, in the plate and shell also, we could constrain out the corresponding eight variables, as shown in Figure 11.9.

Razzaque first coded the plate and shell elements which do this, and their performance is perhaps the most impressive on record for elements of general shape. In plate bending and other $C^{(1)}$ problems, we may be nearing the end of the iso-P road.[14,15] (See Figure 11.20.) Yet the patch test is satisfied only with parallelograms. Furthermore, the shell has major defects, despite its superlative performance. The two variables discarded at each midside, a deflection and a rotation, must both be in carefully defined directions. The three midside variables that are left are equally critical. (In his test problems[16] Razzaque redefined the directions within each element, ignoring any small inconsistencies between neighbouring elements. It would appear likely that he could take this liberty only because of the simple geometry of his test examples. Certainly he could not have expected success in a shell with sharp corners and multiple junctions.)

11.3.7 The ISOBEND plate bending element

The ISOBEND plate bending element has the same nodal variables, but it uses different constrains. In consequence, the patch test now succeeds with *quadrilateral* elements. We learnt the crucial lessons from SemiLoof, so historically this was not a precursor. However, it should have been, and it certainly provides a useful teaching link at this point. (At the time of going to press it is still a relatively untried element, although the program is working and will be made freely available.)

In Reference 1 the idea was mooted of treating a typical side, like AB in Figure 11.9, as a thin beam. In other words, we should impose the displacement and slope at the midside that a thin beam would have experienced. At least, this was the thought. In fact, we put $\gamma_{YZ} = 0$ at the two Gauss points along the side, i.e. at the Loof nodes. This is tantamount to introducing a thin beam as a control along each side, merely to dictate the behaviour of that side. (See Figure 11.10 and note that Y lies along the boundary in the present context.) Such constraints make sense even on curved boundaries.

By choosing a constraint which relates to a *side* rather than to an *element*, we can ensure that the discarded degree of freedom takes the same constrained

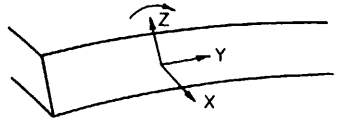

Figure 11.10 In the subsequent discussion, this is the local system of axes at a Loof node

value in the neighbouring element. Because continuity is thus guaranteed, the constraint does not destroy the patch behaviour, provided this is consistent with the constraint.

Unfortunately, if we want the element to succeed in the *quadrilateral* patch test, we must now introduce an extra initial degree of freedom, the *bubble function* of Figure 11.11. It is an inescapable requirement that an isolated

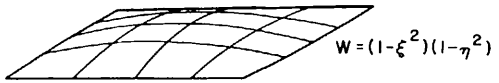

Figure 11.11 The bubble function, an additional degree of freedom, resembles a bubble under constant pressure. It must be added, if the patch test is to be satisfied for quadrilateral elements

element must be able to respond with w = quadratic in x, y. A quadrilateral element gives, for example,

$$x = A + B\xi + C\eta + D\xi\eta$$

On expanding $w = x^2$ we find the term $D^2\xi^2\eta^2$, which is not present amongst the eight terms of the corner–midside functional basis. (Nor, incidentally, is it present in the basis for the Loof functions, whose ninth term $\xi\eta(\xi^2 - \eta^2)$ is different again.)

We therefore add to the Ahmad plate of Figure 11.6 a twenty-fifth degree of freedom, $w = (1 - \xi^2)(1 - \eta^2)$, to make the missing term available. It would be possible to keep this bubble function as a degree of freedom, but we prefer to constrain it out. Observing from Figure 11.11 that at all points around the boundary, except the corners, the normal slope directed inwards is positive, we choose as the constraint:

$$\int (\text{thickness})\gamma_{xz}\, \text{d(boundary)} = 0 \qquad (11.4)$$

This is our first encounter with a discrete Kirchhoff constraint that does not merely put the shear strain zero at some *point* in the element. Yet we should indeed be fortunate if so simple a technique sufficed in every case! We note in passing that if $\gamma_{xz} = \gamma_{yz} = 0$ everywhere, as it must in the patch test, this constraint too is zero. That is, it does not conflict with our patch test requirements.

There are several ways of regarding this constraint, and we mention only the simplest here. It was not whimsical to include the thickness in (11.4); anyway, it is a constant in the patch test. Multiplying (11.4) by the shear modulus, G, or strictly $\frac{5}{6}G$, we get the *total shear force* acting on the element boundary, which is precisely zero in a patch test, and relatively small in any case. We shall amplify this discussion later.

Note A theoretical problem, although not a pressing one, remains. The list of crimes which can be pardoned by the patch test does not, at the moment, include discrete Kirchhoff. So a mathematician would perhaps reject our 'proofs' of convergence, even the patch tests run on the computer, although they will certainly satisfy the engineer.

11.4 Some general remarks on constraints

We must caution the reader against jumping to premature conclusions where constraints are concerned. It is not always straightforward even to count them! Figure 11.8 showed that the thin Ahmad plate with 2 × 2 integration gave only one kinematic degree of freedom per element. The next version, with constraints at the 2 × 2 Gauss points, gave five per element. This was evidently possible because the constraints allowed nonconformity between elements. But then came ISOBEND, with shear constraints at the Loof nodes, which imposed strict conformity and yet *still* gave five degrees of freedom per element. The problem goes, eventually, when we appreciate that a constraint along a side is really imposed only once, not once for each element sharing the side—even if we do have to perform the arithmetic twice. Evidently the subject of constraints is non-trivial.

We have neglected to mention the traps for the unwary: often, the proposed constraints do not register as independent, when we actually try to impose them.[2] But there are easy gains for the enterprising, too. For example, we have made the shears zero. It may be equally worthwhile to impose constraints which seek to make the shears constant, or the bending moments linear.[2] Such possibilities will suggest themselves to any lively mind. To be acceptable, (a) the constraints must be independent, (b) the patch performance should not be of the kind one wants to conceal and (c) rigid-body motion must be respected in all cases.

11.5 The unconstrained displacements of SemiLoof

There is a great deal that is new in the formulation of SemiLoof. We have discussed the precursors, in order to introduce each feature as gently as possible. In one respect, however, there is no precursor known to the author. In SemiLoof the rotations are all applied at different points from the displacements. There are, thus, two families of shape functions: the corner–midside[17] family $N_i(\xi, \eta)$, i = 1 to 8; and the Loof[4] family, $L_j(\xi, \eta)$, j = 1 to 9; not to mention the bubble function. The formulae for L_j have not been published explicitly. For example, the function shown in Figure 11.2 is

$$L_5 = \tfrac{3}{32}(3\eta^2 - \xi^2) + \frac{1}{8}\left[3\eta(1 - \xi^2) + \sqrt{3}\,\xi\left\{3\eta^2 + \eta - 1 + \frac{3\eta}{2}(\eta^2 - \xi^2)\right\}\right]$$

Observe that the basis comprises 1, ξ, η, ξ^2, $\xi\eta$, η^2, $\xi^2\eta$, $\xi\eta^2$ and $\xi\eta(\xi^2 - \eta^2)$—the last term is a peculiar one.

Before applying the constraints, then, we have the displacement at a point on any membrane in the SemiLoof element as the sum of three types of contributions:

(1) *The displacements at the midside and corner nodes* u, v, w cause translations of the eight rigid lines shown in Figure 11.6 without rotations. We have twenty-four degrees of freedom so far.
(2) *The rotations at the Loof and central nodes* introduce a difference in displacement between upper and lower surface. This adds a further eighteen degrees of freedom.
(3) A single *bubble function*, as shown in Figure 11.11, is taken in a direction normal to the element at its centre, $\xi = \eta = 0$. The purpose is again to make it possible for quadrilaterals to pass the patch test.

11.6 The shear constraints for SemiLoof

These forty-three degrees of freedom must now be reduced to thirty-two: we need eleven constraints. The nine already discussed for ISOBEND are still suitable, so that two new constraints are needed. The eleven constraints fall tidily into the following three classes.

1. The eight unwanted rotations at the Loof nodes The slope of the normal in the direction shown in Figure 11.10 generates a shear strain γ_{YZ}. Therefore it is natural to constrain it by putting $\gamma_{YZ} = 0$. (It is, in fact, very natural. These eight shears at the Loof nodes are related to the unwanted rotations by very nearly a diagonal matrix. Moreover, the most obvious alternative constraints, $\gamma_{XZ} = \gamma_{YZ} = 0$ at the 2×2 Gauss points, are not independent.) Let us consider the *patch test*, as it affects the membrane at the level ζ to $\zeta + d\zeta$. Again we perturbate the 'internal' nodes (those which are completely surrounded by elements—see Reference 1) and enquire whether non-zero work is done in a field of constant plane stress. At the Loof nodes A and B in the plan view of the patch, Figure 11.12, the lateral deflections W are identical for neighbouring

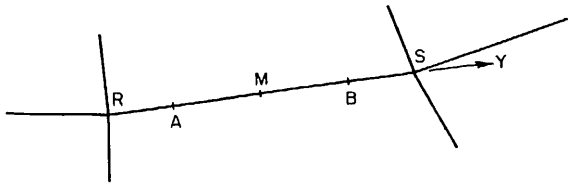

Figure 11.12 A plan view of a pair of neighbouring elements in a patch test to show that a membrane not in the mid-surface conforms at the Loof nodes A and B

elements. Furthermore, the in-plane deflection U normal to RS is controlled by the normal slopes at A and B, which are the unknown nodal variables.

We can now argue that the deflections V along RS are also identical for the neighbouring elements at A and at B, because W_R, W_S and W_M are identical, because W varies quadratically with Y and because the shear γ_{YZ} is constrained to zero at A and at B. It follows that a patch test will succeed, whatever three final constraints are chosen.

2. The two rotations at the centre: Preliminary observation Assume a plate in plane XY has lateral shears γ_{XZ} and γ_{YZ}. If axis Z is fixed and axes X and Y are rotated, the quantity

$$\gamma = \hat{\mathbf{X}}\gamma_{XZ} + \hat{\mathbf{Y}}\gamma_{YZ}$$

transforms as a vector in the plane XY.

The constraints. We store the unit vectors $\hat{\mathbf{X}}_9$ and $\hat{\mathbf{Y}}_9$ at the centre, $\xi = \eta = 0$. We then put

$$\int \hat{\mathbf{X}}_9 \cdot \gamma \, d(\text{area}) = \int \hat{\mathbf{Y}}_9 \cdot \gamma \, d(\text{area}) = 0 \qquad (11.5)$$

and we integrate over the area using the 2×2 Gauss points.

Note that there was a simpler version, when we constrained merely the two shears at the centre. Certainly the patch test was satisfied, but the element behaved far too flexibly in fields of varying stress. In a similar way we recognize that the quadratic beam element of Figure 11.13(c), which also has a central shear constraint, is too flexible; presumably it is the same sort of effect.

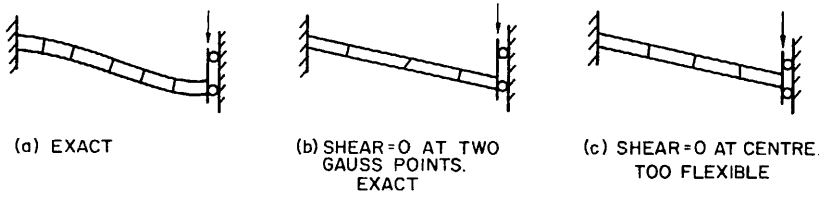

Figure 11.13 A beam under a shear force, with discrete Kirchhoff assumptions, suggests why the central shear constraint gave an over-flexible response in an early experiment with SemiLoof

3. The bubble function $(1 - \xi^2)(1 - \eta^2)$ *(as shown in Figure 11.11)* We observe that it has negative curvature in both the ξ and η directions. So it seems highly probable that the total curvature $\partial^2 W/\partial X^2 + \partial^2 W/\partial Y^2$ is negative almost everywhere. As there is no rotation, $U = V = 0$. The shear corresponding to slope W_X is $\gamma_{XZ} = W_X + U_Z$, so that the expression in the shears that corresponds to the total curvature, in the same way, is

$$\frac{\partial \gamma_{XZ}}{\partial X} + \frac{\partial \gamma_{YZ}}{\partial Y} = \nabla \cdot \gamma \qquad (11.6)$$

It would be reasonable to integrate $\nabla \cdot \gamma$ over the area, to generate an appropriate constraint:

$$\int \nabla \cdot \gamma \, \mathrm{d(area)} = 0 \tag{11.7}$$

This was the constraint originally used in SemiLoof. However, if the thickness is constant, we can transform (11.7) into (11.4) by Green's theorem. In fact, (11.4) is the constraint we now use, as in ISOBEND. Happily, the approach has become simpler with elapsed time.

11.7 Geometric assumptions and modifications in SemiLoof

In this section we shall discuss how only particular geometries of the element permit rigid-body motions. This will lead us to a technique for doctoring the geometry of a new element, very slightly, as a part of the campaign to provide exact rigid-body motions.

The following geometric assumptions are traditional in thin shell models like SemiLoof.

(1) All lines ξ = constant, η = constant, are normal to the mid-surface. Thus, the elements cannot fit together exactly at 'rooftop' junctions.
(2) The shell is so thin that the element of surface d(area) for all membranes may be treated as equal to that for the mid-surface.
(3) The membranes are nearly parallel.

But we have given ourselves a difficult assignment and traditions (1) and (3) must go. We have already satisfied the patch test for quadrilaterals. A twin principle now dominates; henceforth, we require that no *assemblage* of elements violates the rigid-body motions. (In Reference 2 this requirement was overlooked.) We must bear in mind two relevant propositions:

(a) Strict iso-P elements will provide the rigid-body motions.
(b) A pair of elements will provide a rigid-body motion *only if* the nodal variables tying them together (the rotations in particular) are defined *consistently* by the rigid-body motion.

When we first encounter a curved element, we must work through several stages of calculation, in order to create a geometry that permits rigid-body motions.

Stage 1 We interpolate the given scalar thicknesses at the corner and midside nodes, T_i, $i = 1$ to 8, to generate the values T_j, $j = 1$ to 9, at the Loof and central nodes. We then erect the vector thicknesses, $\mathbf{T}_j$ to a first approximation, normal to the mid-surface. (A vector thickness is defined as the rigid line ξ = constant, η = constant, terminated at $\zeta = \pm 1$.)

Stage 2 To ensure that we have an iso-P element, the geometry must be such that it could have come from $\mathbf{T}_i$, eight of them, at the corners and midsides,

even though in fact we have *nine* $\mathbf{T}_j$ at the Loof nodes. It is not too difficult to derive the condition that $\mathbf{T}^* = \sum \mathbf{T}_j^* L_j$, $j = 1$ to 9, uses only the *eight* polynomial terms, where we have now modified $\mathbf{T}_j$ to $\mathbf{T}_j^*$; note that the central node, $j = 9$, is not involved.

$$\sum_1^8 (-1)^j \mathbf{T}_j^* = 0$$

Proof. Consider nodes A and B in Figure 11.12, where $\xi = \pm\sqrt{\frac{1}{3}}$ respectively. If we postulate that u is a polynomial in the corner–midside basis, then u varies quadratically with ξ along RS. It follows that

$$u_S - u_R = \sqrt{3}(u_B - u_A)$$

If the Loof nodes are A, B, C, D... anticlockwise, and the corner nodes are R, S, T, U, we can write

$$(u_S - u_R) + (u_T - u_S) + (u_U - u_T) + (u_R - u_U) = 0$$
$$= \sqrt{3}[(u_B - u_A) + (u_D - u_C) + (u_F - u_E) + (u_H - u_G)]$$

(Alternatively, we can get this result by writing the 9×8 matrix giving the values at the Loof nodes in terms of those at the corner–midside nodes. We can then show that the relevant 8×8 partition has rank 7; the above result appears as a byproduct. This alternative approach does nothing to ease the paper shortage.)

However, $\mathbf{T}_j^*$ will now be only approximately normal to the mid-surface. We must also insist that the vector thicknesses at the Loof nodes shall possess zero component along the boundary. For otherwise a rotation $\boldsymbol{\Omega}$ normal to the tangent plane, as in Figure 11.14, would cause a relative movement into and out of the paper, which would have every appearance of a rotation about $\hat{\mathbf{Y}}_j$.

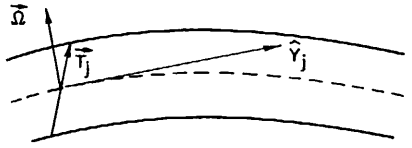

Figure 11.14 The vector thickness at a Loof node must have zero component along the edge, to avoid spurious rotations

To avoid such spurious rotations we must adjust the initial normal thicknesses $\mathbf{T}_j$ so as to satisfy this condition also. We note that such artificial modifications will be small, i.e. of the same order of magnitude as the variations of normal thickness in a 'constant thickness' iso-P element of similar curvature. Let us then assume that

$$\mathbf{T}_j^* = \mathbf{T}_j - (-1)^j(\mathbf{p} - \mathbf{p} \cdot \hat{\mathbf{Y}}_j \hat{\mathbf{Y}}_j), \qquad j = 1 \text{ to } 8 \tag{11.8}$$

is the corrected version. For if $\mathbf{T}_j$ has zero component along $\hat{\mathbf{Y}}$, then so has $\mathbf{T}_j^*$,

whatever value **p** may have. We now premultiply by $(-1)^j$ and add, and thus we find the equation for **p**.

$$\sum_1^8 (-1)^j \mathbf{T}_j^* = \sum_1^8 (-1)^j \mathbf{T}_j - \sum_1^8 (\mathbf{p} - \mathbf{p} \cdot \hat{\mathbf{Y}}_j \hat{\mathbf{Y}}_j) = 0 \tag{11.9}$$

Observe that $\mathbf{T}_9$, the central thickness, is unchanged. Translating this equation into matrix notation,

$$\left[8\mathbf{I} - \sum_1^8 \hat{\mathbf{Y}}_j \hat{\mathbf{Y}}_j^{\mathrm{T}}\right]\mathbf{p} = \sum_1^8 (-1)^j \mathbf{T}_j \tag{11.10}$$

Other techniques are possible, but this one is numerically stable because the 3×3 matrix is positive definite.

Stage 3 We construct and reduce the constraint matrix. Here the measure of shear strain must respect rigid-body motions, or they will be destroyed; this is discussed in the next section.

Stage 4 We use the constraint matrix to combine the virgin shape functions and their derivatives at a given point (ξ, η). If the element geometry is not new, so that the preliminary work is already done, then we can enter at Stage 4. The routine tests for this at every entry, so as to avoid unnecessary work.

11.8 Shell theory: Strain definitions

The formulae that will lead us from the shape function derivatives to the bending and lateral shear strains seem to the author neither simple nor obvious. These definitions of strain may well be the starting point for future elements derived from Ahmad's: they could be important in themselves. Perhaps to call them a 'shell theory' seems pretentious at first—as Morley has pointed out, conventional shell theories have taken over half a century to mature—yet the description fits. Once again the aim is to simplify the calculations without introducing unacceptable errors.

We wished to satisfy two requirements, (a) that the bending behaviour of flat uniform plates was reproduced and (b) that rigid-body motions should give zero strains *exactly*. To this end we added one correction term after another, until the computer finally registered success. At this stage it was easy to confirm the formulae algebraically. Such a procedure hardly guarantees uniqueness, but a unique shell theory is perhaps a contradiction in terms.

This Ahmad shell theory is contained in the two equations:

$$\begin{bmatrix}\gamma_{XZ}\\ \gamma_{YZ}\end{bmatrix} = \begin{bmatrix}W_X\\ W_Y\end{bmatrix} + \frac{1}{T}\Delta \cdot \begin{bmatrix}\hat{\mathbf{X}}\\ \hat{\mathbf{Y}}\end{bmatrix} - \frac{1}{T}\begin{bmatrix}U_X & U_Y\\ V_X & V_Y\end{bmatrix}\begin{bmatrix}R\\ S\end{bmatrix} \tag{11.11}$$

$$\begin{bmatrix}U_{XZ} & V_{XZ}\\ U_{YZ} & V_{YZ}\end{bmatrix} = \frac{1}{T}\begin{bmatrix}\Delta_X\\ \Delta_Y\end{bmatrix} \cdot [\hat{\mathbf{X}}\ \hat{\mathbf{Y}}] - \frac{1}{T}\begin{bmatrix}R_X & S_X\\ R_Y & S_Y\end{bmatrix}\begin{bmatrix}U_X & V_X\\ U_Y & V_Y\end{bmatrix} + \frac{1}{T}\begin{bmatrix}T_X\\ T_Y\end{bmatrix}[W_X\ W_Y] \tag{11.12}$$

which we shall now explain, derive and justify. As before, Z is any axis normal to the mid-surface and $\hat{\mathbf{Z}}$ is the corresponding unit normal.

X and Y would be, respectively, the outward-pointing normal and the axis along the boundary, as in Figure 11.10. But for points inside the element, X and Y may be any directions perpendicular to Z.

N_i will be the eight corner–midside shape functions, and L_j will be the nine Loof shape functions as before; these do not occur explicitly in the formulae.

U, V and W are the deflections in the X, Y and Z (local) directions. Thus, a vector displacement $\mathbf{d}_i$ at a node would cause a displacement $N_i\mathbf{d}_i$ at some other point, which using the scalar product gives $U = (\mathbf{d}_i \cdot \hat{\mathbf{X}})N_i$, for example, as the resolute in the X direction.

U_X for example denotes $\partial U/\partial X$: thus

$$U_X = \sum_1^8 (\mathbf{d}_i \cdot \hat{\mathbf{X}}) \frac{\partial N_i}{\partial X} \tag{11.13}$$

We calculate the shape function derivatives $\partial N_i/\partial X$ and $\partial N_i/\partial Y$ from (11.2) and the program uses them extensively, (see Appendix). In that expression, ξ and η were the covariant base vectors. If x, y, z are the global axes we have, for example,

$$\xi = \frac{\partial(x, y, z)}{\partial \xi} = \sum_{i=1}^8 (x_i, y_i, z_i) \frac{\partial N_i}{\partial \xi} \tag{11.14}$$

In the same way, Δ is the difference due to rotations in the displacements at A and B as in Figure 11.15, which are corresponding points (ξ, η) lying on the top and bottom surfaces; so that $\Delta = \sum L_j \Delta_j$, and for example

$$\Delta_X = \sum_{j=1}^9 \Delta_j \frac{\partial L_j}{\partial X} \tag{11.15}$$

The vector thickness $\mathbf{T}^*$ in an Ahmad shell is in general not normal to the mid-surface, as we have seen. In terms of base vectors, as in (11.15), we should write $\mathbf{T}^* = 2\zeta + \sum L_j \mathbf{T}_j^*$. Thus we can find the resolutes R, S and T so that

$$\mathbf{T}^* = R\hat{\mathbf{X}} + S\hat{\mathbf{Y}} + T\hat{\mathbf{Z}} \tag{11.16}$$

Note that T, a scalar, is the normal resolute of $\mathbf{T}^*$, the vector, as in Figure 11.15. Note also, that T is not exactly what we should get by interpolating the original thicknesses T_i as input at corners and midsides. Quantities like R_X are again calculated using the local shape function derivatives $\partial L_j/\partial X$.

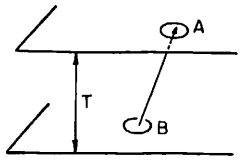

Figure 11.15 In assessing the bending stresses, we compare the membrane actions at B with those at A, not always directly beneath B. But T denotes the normal thickness, not the length AB

There will be no need for second derivatives: this desirable feature of the original Ahmad shells is inherited by the present shell theory. If the Kirchhoff assumption that normals remain normal were enforced everywhere, the following would be exactly equivalent:

$$\left.\begin{aligned} &-U_{XZ} \text{ instead of the curvature, } W_{XX} \\ &-U_{YZ} - V_{XZ} \text{ instead of the twist, } 2W_{XY} \\ &-V_{YZ} \text{ instead of the curvature, } W_{YY} \end{aligned}\right\} \tag{11.17}$$

Scalar products occur extensively in the shape function subroutine. Notice especially the first term on the right-hand side of (11.12), which uses the dot product between two matrices whose terms are vectors.

11.9 Derivation of the shell equations

The formulae (11.11) and (11.12) evolved piecemeal, in response to a pressing need. Doubtless future workers will find a synthetic approach and the Ahmad model will acquire some respectability. Already the model seems intrinsically simpler than classical shell theories, at least for small deflections.

We now describe how the various terms came to be added. Thus, the first two terms of (11.11) clearly represent, e.g., $\gamma_{XZ} = W_X + U_Z$. The third term corrects for those spurious shear strains which arise when A is not orthogonally above B, as in Figure 11.15. For example, if the plate is rotated about Z, then A moves relative to a position directly above B and this looks like a shear strain. Again, if the plate is stretched horizontally, then the angle between AB and the true normal increases. So far, the measure of shear only compares the movements of A and B, so that a correction is needed.

To treat this more formally, we write the operator:

$$\frac{\partial}{\partial\zeta} = \frac{1}{2}\left[R\frac{\partial}{\partial X} + S\frac{\partial}{\partial Y} + T\frac{\partial}{\partial Z}\right] \tag{11.18}$$

for both sides of the equation give the change in going from the central to the top surface. It follows that

$$\frac{\partial}{\partial Z} = \frac{1}{T}\left[2\frac{\partial}{\partial\zeta} - R\frac{\partial}{\partial X} - S\frac{\partial}{\partial Y}\right] \tag{11.19}$$

For example, in computing $\gamma_{XZ} = W_X + U_Z$ the first term needs no correction; the second and third terms of (11.11) represent U_Z as calculated from (11.19).

The bending strains are less straightforward. For a start, when we say U_{XZ} for example, what we really mean is that we take U_X both at A and at B (which is not directly below A) and we divide the difference by T, the normal thickness.

This procedure fails, not for the obvious reason that A is not directly above B, but because a strain or rotation of the mid-surface causes a spurious bending strain. The first correction arises from considering a tapering plate, i.e. T varies with X and Y. Let us set up our X, Y axes at B, rather than at the mid-surface.

Then the direction normal to the membrane at A will be $[-T_X, -T_Y, 1]$. Hence a normal deflection W at B will have the additional components, as measured in the X, Y axes at A, of $\delta U = T_X W$, $\delta V = T_Y W$. Thus, for example, U_{XZ} acquires the term $T_X W_X/T$. Similarly U_{YZ} acquires the term $T_X W_Y/T$. (If we put the latter term in V_{XZ} instead, it is for the sake of tidiness rather than for any significant principle. We always add U_{YZ} to V_{XZ}, as in (11.17), so that it never makes any difference to our final calculations. The only advantage is that the formula as modified in (11.12) gives $U_{YZ} = V_{XZ} = 0$ for a rigid-body motion, whereas without the change $U_{YZ} = -V_{XZ}$ and is non-zero.)

The second and last correction arises because a pure displacement $\mathbf{d}_i$ (with all $\boldsymbol{\Delta}_j$ zero) causes the same $\partial\mathbf{d}/\partial\xi$ for example at A as at B; but the transformation into $\partial/\partial X$ and $\partial/\partial Y$ is slightly different. This causes a spurious bending term, especially when the element is highly curved. For a point (X, Y) at A would become a point $(X + R, Y + S)$ at B so that, approximately:

$$\begin{bmatrix} dX \\ dY \end{bmatrix}_A = \begin{bmatrix} 1 + R_X & R_Y \\ S_X & 1 + S_Y \end{bmatrix}\begin{bmatrix} dX \\ dY \end{bmatrix}_B \tag{11.20}$$

If now we consider the total differential of some function, ϕ:

$$d\phi = [\phi_X \ \phi_Y]_A\begin{bmatrix} dX \\ dY \end{bmatrix}_A = [\phi_X \ \phi_Y]_B\begin{bmatrix} dX \\ dY \end{bmatrix}_B \tag{11.21}$$

We now substitute from (11.20)

$$d\phi = [\phi_X \ \phi_Y]_B\begin{bmatrix} dX \\ dY \end{bmatrix}_B = [\phi_X \ \phi_Y]_A\begin{bmatrix} 1 + R_X & R_Y \\ S_X & 1 + S_Y \end{bmatrix}\begin{bmatrix} dX \\ dY \end{bmatrix}_B \tag{11.22}$$

so that

$$\begin{bmatrix} 1 + R_X & S_X \\ R_Y & 1 + S_Y \end{bmatrix}\begin{bmatrix} \phi_X \\ \phi_Y \end{bmatrix}_A = \begin{bmatrix} \phi_X \\ \phi_Y \end{bmatrix}_B$$

and

$$\begin{bmatrix} \phi_X \\ \phi_Y \end{bmatrix}_A - \begin{bmatrix} \phi_X \\ \phi_Y \end{bmatrix}_B = -\begin{bmatrix} R_X & S_X \\ R_Y & S_Y \end{bmatrix}\begin{bmatrix} \phi_X \\ \phi_Y \end{bmatrix}_A \tag{11.23}$$

Thus, for example, U_{XZ} acquires the extra term $-(R_X U_X + S_X U_Y)/T$.

The arguments behind both these bending corrections involve approximations. However, the computer now gives exact rigid-body motions, so that the practical task is complete.

Note In ISOBEND we need just one of these corrections: the last term of (11.12) involving T_X and T_Y. Without this term, rigid-body motions would not be exact.

11.10 Theoretical justification of the shell equations

This section is mandatory; nevertheless it will be fruitless unless the justification gives us a deeper understanding, and maybe a hint leading to some synthetic approach—which it does not do at the time of writing. The task falls into two parts. In the first, we merely record that in the case of an Ahmad plate of uniform thickness, with ζ normal to the plate, the correction terms all vanish. Thus the bending of flat uniform plates remains 'uncorrected', as we wished.

The second part is, however, quite challenging. At least we can again quickly dispose of the easy case: in a rigid-body translation, U, V and W are constant, so that their X and Y derivatives are zero. Also Δ and its derivatives are zero. Thus every term in (11.11) and (11.12) is zero.

This brings us to the *rigid-body rotations*. Let us start with $\boldsymbol{\Omega} = \hat{\mathbf{X}}$ in the lower surface, so that $V = -Z$ and $W = Y$, where X, Y and Z are measured from A. Thus Δ, as used in the formulae, is $-T\hat{\mathbf{Y}} + S\hat{\mathbf{Z}}$. Substituting in (11.11) we have

$$\begin{bmatrix}\gamma_{XZ}\\ \gamma_{YZ}\end{bmatrix} = \begin{bmatrix}0\\ 1\end{bmatrix} + \frac{1}{T}\begin{bmatrix}0\\ -T\end{bmatrix} - \frac{1}{T}\begin{bmatrix}0 & 0\\ 0 & 0\end{bmatrix}\begin{bmatrix}R\\ S\end{bmatrix} \tag{11.24}$$

which is identically zero. Substituting now in (11.12):

$$\begin{bmatrix}U_{XZ} & V_{XZ}\\ U_{YZ} & V_{YZ}\end{bmatrix} = \frac{1}{T}\begin{bmatrix}0 & -T_X\\ 0 & -T_Y\end{bmatrix} - \frac{1}{T}\begin{bmatrix}R_X & S_X\\ R_Y & S_Y\end{bmatrix}\begin{bmatrix}0 & 0\\ 0 & 0\end{bmatrix} + \frac{1}{T}\begin{bmatrix}T_X\\ T_Y\end{bmatrix}[0\ \ 1] \tag{11.25}$$

which again, is identically zero.

Putting $\boldsymbol{\Omega} = \hat{\mathbf{Y}}$ would give similar results; but the case with $\Omega = \hat{\mathbf{Z}}$ is different and must be checked. Here we have $U = -Y$ and $V = X$ in the lower surface, X and Y being measured from B. Hence in the upper surface $U = -(Y + S)$ and $V = X + R$, measuring X and Y from A, which gives $\Delta = -S\hat{\mathbf{X}} + R\hat{\mathbf{Y}}$. Substituting in (11.11) we have

$$\begin{bmatrix}\gamma_{XZ}\\ \gamma_{YZ}\end{bmatrix} = \begin{bmatrix}0\\ 0\end{bmatrix} + \frac{1}{T}\begin{bmatrix}-S\\ R\end{bmatrix} - \frac{1}{T}\begin{bmatrix}0 & -1\\ 1 & 0\end{bmatrix}\begin{bmatrix}R\\ S\end{bmatrix} \tag{11.26}$$

and this is identically zero. Finally, substituting in (11.12) gives

$$\begin{bmatrix}U_{XZ} & V_{XZ}\\ U_{YZ} & V_{YZ}\end{bmatrix} = \frac{1}{T}\begin{bmatrix}-S_X & R_X\\ -S_Y & R_Y\end{bmatrix} - \frac{1}{T}\begin{bmatrix}R_X & S_X\\ R_Y & S_Y\end{bmatrix}\begin{bmatrix}0 & 1\\ -1 & 0\end{bmatrix} + \frac{1}{T}\begin{bmatrix}T_X\\ T_Y\end{bmatrix}[0\ \ 0] \tag{11.27}$$

which is again identically zero. This proves the adequacy but not, observe, the uniqueness of the shell theory. Computer checks for correctness have also confirmed the theory, so the stage has been reached to discuss the present implementation and the performance of the element in practice.

11.11 The implementation of SemiLoof

In the author's view, the coding of a new element is work that should not be delegated. In the first place, the question of whether a particular approach leads to good code is a vital one in choosing between rival formulations. In the second place, the coding should be done well. The probability of errors creeping in, and causing trouble later, depends on the number and length of the statements, as does the storage capacity required. Furthermore, the coding is the one unambiguous statement of the algorithm itself; it should be scrupulously accurate and should ideally form part of the publication; furthermore, it should be transparent and well documented.

The shape function package for SemiLoof is available. With good documentation and eleven diagnostic checks, it is easy to implement. The 440 FORTRAN statements compile into a program of 70 000 bits on the Swansea ICL computer. In addition, it requires 1740 real words of working storage. The speed could undoubtedly be improved: the program suffered continual change over the gestation period of fourteen months or so and clarity was the main objective throughout that time.

Rank and spurious mechanisms

Ideally the stiffness matrix for a quadrilateral element would have a rank of 26 = 32 (the number of nodal variables) − 6 (the number of rigid-body motions available); a triangle, 18 = 24 − 6. But each integrating point can contribute at most six (the rank of the modulus matrix). This gives a maximum rank of 24 for the quadrilateral, using 2 × 2 integration, or of 18 for the triangle using the midside rule. Therefore the quadrilateral must have at least two spurious mechanisms, like those illustrated in Figure 11.16 for a flat rectangular element.

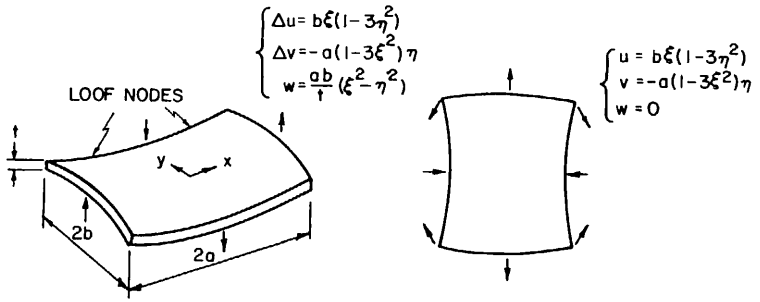

Figure 11.16 With 2 × 2 integration, we have these two extra zero-energy modes in a rectangle: the first represents spurious bending, the second, spurious membrane action

(Experience has not so far revealed further spurious mechanisms, either for the triangle or for the quadrilateral.) Such mechanisms can clearly propagate

through neighbouring elements and hence infect the whole field. We can:

(a) Understand the danger and hence avoid it, at any rate in small problems. But with very fine meshes there may be a tendency for such noise to grow as one moves away from any fixed boundary.
(b) Use triangles. But this invokes more assembled variables and gives about fives times the errors!
(c) Use a higher integration rule. This seems to dispose of the mechanisms, but at the cost of increased computing time and of rather untidy programming. The rule currently being tried introduces a fifth point, with some arbitrary small weighting:

$$\int_{-1}^{1}\int_{-1}^{1} \phi(\xi,\eta)\,d\xi\,d\eta = 0{\cdot}2\phi(0,0) + 0{\cdot}95\sum_{1}^{4}\phi(\pm 0{\cdot}592348878,\ \pm 0{\cdot}592348878)$$

The final answers are somewhat worse in small problems. This formula integrates $1, \xi^2, \eta^2$ correctly, but not $\xi^2\eta^2$, so that the patch performance is unchanged: constant stresses are reproduced exactly with quadrilateral geometry. However, we are not entirely happy with this technique. Razzaque has found the 3×3 rule more satisfactory.
(d) Possibly, by adapting the technique for discovering rank, take the stiffness matrix with 4-point integration, together with the six rigid-body modes, and generate numerically the nodal components for the two mechanisms, say v_1 and v_2. We could then replace $\mathbf{K}$ by $\mathbf{K} + \alpha_1\mathbf{v}_1\mathbf{v}_1^T + \alpha_2\mathbf{v}_2\mathbf{v}_2^T$, where α_1 and α_2 would depend on the thickness, etc. The trouble here is that we cannot at present relate the technique to the patch test.

The performance is better than was expected. Speculative trials, first in the beam of Reference 2, and later in the shell element, showed that very deeply curved geometry is acceptable. Indeed, the diagnostics in the program now allow the nodal normals to deviate from each other by 60°, and the results remain good.

Provided that the user can accept stress values at the 2×2 Gauss points, remarkably coarse meshes frequently give adequate engineering accuracy. For example, the uniformly loaded encastré disc of Figure 11.17 with $\nu = 0{\cdot}3$ gives stresses all within ± 3 per cent of the largest stress. Again, the square

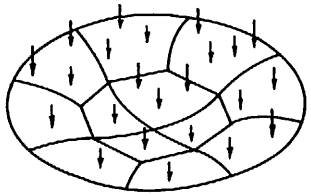

Figure 11.17 A uniformly loaded circular plate gives excellent results

plate of Figure 11.18 with uniform loading gives a central deflection +0·013 per cent in error. (This sort of performance, it is suggested in Reference 2, tempts us to surmise that we might have an element suitable for minicomputer operation in the near future. The typical casual user would be an ordinary designer, interested in some design detail and willing to use up to about 8 or 10 elements.)

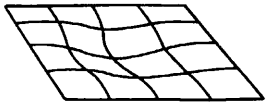

Figure 11.18 Similarly, a uniformly loaded square plate shows SemiLoof as a highly competitive performer

Similar accuracy is available with curved shells. Perhaps the most spectacular example was that shown in Figure 11.19. Analytically it is trivial; but as a test of a general shell element it is not, for these elements all subtend 60° and three-quarters of the strain energy is in bending. The stresses are accurate to 1 per cent.

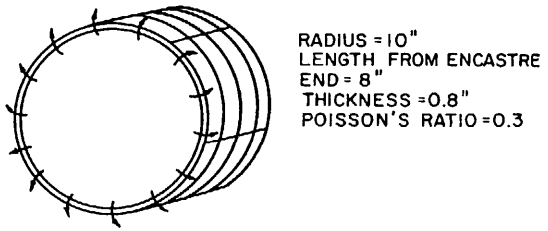

Figure 11.19 These elements subtend 60° at the centreline. Comparing with the exact solution, which contains terms like $e^{-\lambda x}\sin\lambda x$, each element covers a step of 0·9 in λx

The response of a square plate to a point load, as plotted in Figure 11.20, is less gratifying, being much worse than in Reference 18. This may be because the corners can hinge, as illustrated in Figure 11.21. If so, it might be an inevitable consequence of the nodal configuration chosen: one surmises that the element of Reference 15 has the same fault. Perhaps, indeed, such behaviour will be acceptable, because in practice a point load is usually taken by a beam. Anyway, most loads are distributed. When we do have intense local loading, we should refine the mesh to catch the high stresses. (Indeed, it can be argued that elements which give good deflections at points of infinite stress are insufficiently alarmist.)

Reference 2 solved a large example, of a curved slab bridge, using 50 elements. Reference 19 analysed a cylinder–cylinder intersection, with very local bending stresses near the join. Meshes with 28, 40 and 60 elements were tried. These larger examples have not yet revealed any difficulties, apart from the universal one of avoiding errors in the data input, and the results have been excellent.

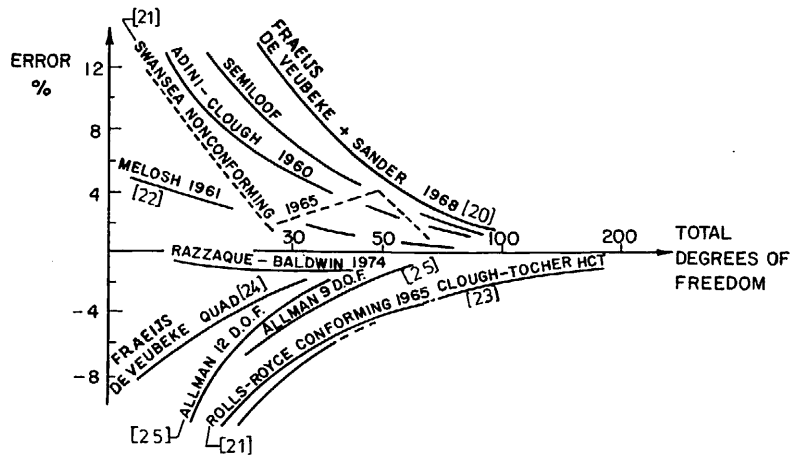

Figure 11.20 A point load is less flattering. Yet SemiLoof is still not much worse than a number of popular elements

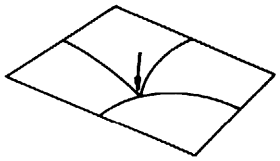

Figure 11.21 This is a plausible explanation of why SemiLoof is too flexible under a point load. There is no corner slope connection, so that it could perhaps hinge quite badly in certain load cases

Many much larger examples have now been run commercially and have given satisfaction.

Appendix

Proof of (11.2). Consider a function ϕ which varies over the surface. Interpret geometrically a change $(\partial\phi/\partial\xi)\,d\xi$. It means that we travel to a point $\xi\,d\xi$ away from our starting point, recalculate ϕ, and find the change. Because $\hat{\mathbf{X}}$ and $\hat{\mathbf{Y}}$ lie in the ξ, η plane, i.e. they are coplanar with ξ and η, we can always write $\xi\,d\xi = \hat{\mathbf{X}}\,dX + \hat{\mathbf{Y}}\,dY$. Because $\hat{\mathbf{X}}$ and $\hat{\mathbf{Y}}$ are mutually perpendicular, we can scalar-multiply the relation by $\hat{\mathbf{X}}$ giving $\xi \cdot \hat{\mathbf{X}}\,d\xi = dX$, and similarly $dY = \xi \cdot \hat{\mathbf{Y}}\,d\xi$. So we can write

$$\frac{\partial\phi}{\partial\xi}\,d\xi = \frac{\partial\phi}{\partial X}\,dX + \frac{\partial\phi}{\partial Y}\,dY$$

(where dX and dY are equivalent to the change $d\xi$)

$$= \frac{\partial\phi}{\partial X}\xi \cdot \hat{\mathbf{X}}\,d\xi + \frac{\partial\phi}{\partial Y}\xi \cdot \hat{\mathbf{Y}}\,d\xi$$

Hence we have the first equation of (11.2), and the second is similar.

References

1. B. M. Irons and A. Razzaque, 'Experience with the patch test', in *The Mathematical Foundations of the Finite Element Method with Applications to Partial Differential Equations*, K. Aziz (Ed.), Academic, London, 1972, pp. 557–587.
2. F. Albuquerque, *A Beam Element for Use with the SemiLoof Shell Element*, M.Sc. thesis, University of Wales, 1973.
3. B. M. Irons, 'Comment on "A higher order conforming rectangular plate element" by S. Gopalacharyulu', *Int. J. Num. Methods in Eng.*, **6**, 305 (1973).
4. H. W. Loof, 'The economical computation of stiffness of large structural elements', *Int. Symp. on Use of Comp. in Struct. Eng.*, University of Newcastle-upon-Tyne, 1966.
5. B. M. Irons, 'The patch test for engineers', paper presented at *Finite Elements Symposium*, Atlas Computing Laboratory, Chilton, Didcot, Berks, 27th March 1974.
6. W. Visser, 'The application of a curved mixed-type shell element', *IUTAM Symp. on High Speed Computing of Elastic Structures*, University of Liège, August 1970, Tome 1, p. 321.
7. S. O. Asplund, *Structural Mechanics: Classical and Matrix Methods*, Prentice-Hall, Englewood Cliffs, N.J., 1966.
8. S. Ahmad, *Curved Finite Elements in the Analysis of Solid, Shell and Plate Structures*, Ph.D. thesis, University of Wales, 1969.
9. R. J. Melosh, 'A flat triangular shell element stiffness matrix', *Proc. of (first) Conf. on Matrix Methods in Structural Mechanics*, AFFDL TR 66-80, Wright-Patterson AFB, Ohio, 1965, p. 503.
10. E. Winkler, *Die Lehre von der Elastizitat und Festigkeit*, Prague, 1867, Ch. 15.
11. J. A. Stricklin, W. E. Haisler, P. E. Tisdale and R. Gunderson, 'A rapidly converging triangular plate element', *AIAA J.*, **7**, 180 (1969).
12. J. Too, *Two Dimension, Plate, Shell and Finite Prism Isoparametric Elements and Their Application*, Ph.D. thesis, University of Wales, Swansea, 1971.
13. S. F. Pawsey and R. W. Clough, 'Improved numerical integration of thick shell finite elements', *Int. J. Num. Methods Eng.*, **3**, 576 (1971).
14. O. C. Zienkiewicz, R. L. Taylor and J. Too, 'Reduced integration technique in general analysis of plates and shells', *Int. J. Num. Methods in Eng.*, **3**, 275 (1971).
15. J. T. Baldwin, A. Razzaque and B. M. Irons, 'Shape function subroutine for an isoparametric thin plate element', *Int. J. Num. Methods in Eng.*, **7**, 431 (1973).
16. A. Razzaque, *Finite element analysis of plates and shells*, Ph.D. thesis, University of Wales, Swansea, 1972.
17. B. M. Irons, 'Engineering application of numerical integration in stiffness methods', *AIAA J.*, **4**, 2035 (1966).
18. B. M. Irons and A. Razzaque, 'A further modification to Ahmad's shell element', *Int. J. Num. Methods Eng.*, **5**, 588 (1973).
19. R. Locke, *An Analysis of an Intersection Problem Using the SemiLoof Shell Element*, B.Sc. thesis, Civil Engineering, University of Wales, Swansea, 1974.
20. B. Fraeijs de Veubeke and G. Sander, 'An equilibrium model for plate bending', *Int. J. Solids Struct.*, **4** (1968).
21. G. Bazeley, Y. Cheung, B. M. Irons and O. C. Zienkiewicz, 'Triangular elements in plate bending—conforming and nonconforming solutions', *Proc. of (First) Conf. on Matrix Methods in Struct. Mech.*, AFFDL-TR-66-80, 1965, p. 547.
22. R. J. Melosh, 'A stiffness matrix for the analysis of thin plates in bending', *J. Aero. Sci.*, **28**, 34 (1961).
23. R. W. Clough and J. Tocher, 'Finite element stiffness matrices for the analysis of plate bending', *Proc. of (First) Conf. on Matrix Methods in Struct. Mech.*, AFFDL-TR-66-80, 1965, p. 515.
24. B. Fraeijs de Veubeke, 'A conforming finite element for plate bending', *Int. J. Solids Struct.*, **4**, 95 (1968).

25. D. Allman, 'Triangular plate element for plate bending with constant and linearly varying bending moment', *Proc. of IUTAM Symp. on High-Speed Computing of Elastic Structures*, Liège, 1970, Tome 1, p. 105.

Chapter 12

Finite Element Analysis of Arch Bridges

A. B. Sabir

12.1 Introduction

A study of the application of the finite element analysis to the stress-analysis of a bridge consisting of a broad circular arch vault and a slab deck is presented. Some possible profiles for the broad arch bridge in which the slab is connected along its mid-section to the crown of the arch vault are shown in Figure 12.1.

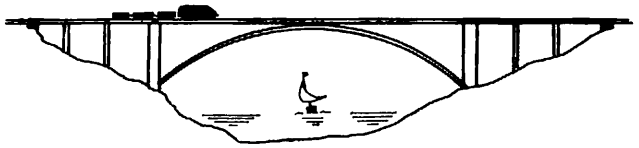

(a)

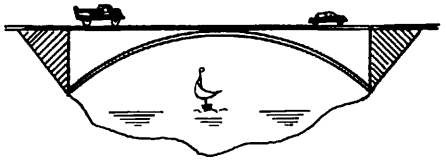

(b)

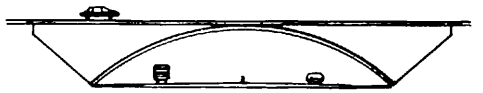

(c)

Figure 12.1 Possible profiles for the broad arch bridge